Lateral Electromagnetic Waves and Pulses on Open Microstrip

RONOLD W. P. KING, LIFE FELLOW, IEEE

Abstract—**The propagation of lateral electromagnetic waves and pulses on microstrip is investigated further. Interference patterns generated by the superposition of the lateral and direct waves along the air–substrate surface are shown. The field generated by the pulse excitation of a horizontal dipole on the air–substrate boundary is shown to consist of a lateral-wave pulse and a slower direct-wave pulse. Their differences in shape and decay rate are clarified. It is shown that the shape of a Gaussian pulse propagating along an open microstrip transmission line is closely related to the shape of the lateral electric-field pulse generated by a Gaussian current pulse in a dipole the air–substrate boundary.**

I. Introduction

IN A RECENT paper [1] the electric field generated by a horizontal electric dipole on the air–substrate boundary of open microstrip (Fig. 1) was calculated from the exact integrals subject to the inequalities

$$k_0^2 < |k_1^2| \ll |k_2^2| \tag{1}$$

where k_0 is the wavenumber of air, k_1 the wavenumber of the dielectric substrate, and k_2 the wavenumber of the conducting base. It was shown that each component of the field consists of two parts: a lateral wave that travels in the air and a direct wave that travels in the substrate. Since the two waves travel with different velocities, viz., $c = 3 \times 10^8$ m/s in the air and $v = c\epsilon_{1r}^{-1/2}$ in the dielectric with the relative permittivity ϵ_{1r}, the superposition of the two must yield interference patterns. Such a pattern was shown [1, fig. 2] for an air-distilled water boundary when the water is a half-space. Since the formulas for the two-layer region [1, eqs. (57)–(59)] are quite similar to those of the three-layer microstrip [1, eqs. (44), (45), and (55)], it was concluded that similar patterns must exist in the microstrip. It is shown below that this is true.

Of considerable interest is the relation between the electromagnetic field generated by a horizontal electric dipole and that of a microstrip transmission line. Each element of current in the stripline corresponds to a horizontal electric dipole and the superposition of contributions from all such elements constitutes the field of the transmission line. The study of this superposition is greatly simplified for single-pulse propagation so that this case is examined in some detail for a Gaussian pulse. The changes in shape attributed to dispersion along the transmission line are shown to correspond closely to the similar changes for the propagation of a lateral-wave pulse.

Manuscript received March 24, 1989; revised July 5, 1989. This work was supported in part by the Joint Services Electronics Program under Grant N00014-89-J-1023 with Harvard University.

The author is with the Gordon McKay Laboratory, Harvard University, Cambridge, MA 02138.

IEEE Log Number 8931563.

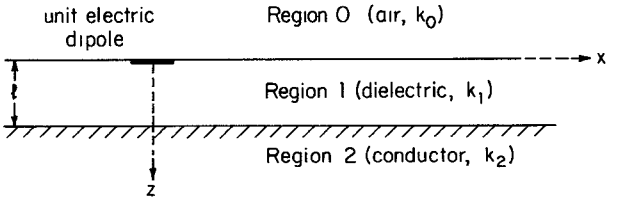

Fig. 1. Unit electric dipole on plane boundary $z = 0$ between air and a sheet of dielectric with thickness l over a conducting ground plane.

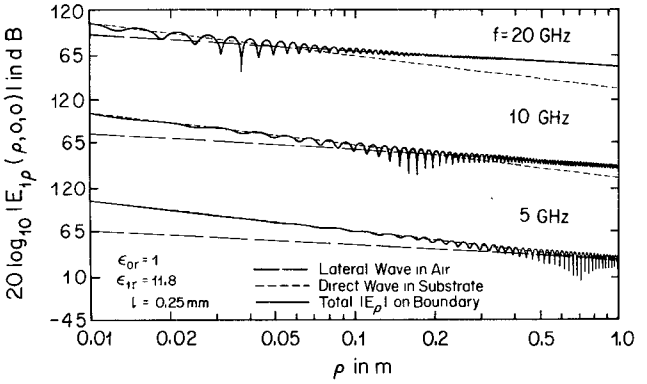

Fig. 2. Interference patterns of lateral- and direct-wave components of E_ρ.

II. Interference Patterns in Microstrip Fields

In order to show actual interference patterns in microstrip, calculations have been made from the complete formulas (44) and (45) in [1] for the components of the electric field tangent to the air–substrate boundary, that is, from the formulas for $E_{1\rho}(\rho,0,0) = E_{2\rho}(\rho,0,0)$ and $E_{1\phi}(\rho,\pi/2,0) = E_{2\phi}(\rho,\pi/2,0)$ on the boundary $z = 0$ between the substrate and the air when the relative permittivity of the substrate is $\epsilon_{1r} = 11.8$ and its thickness is $l = 0.25$ mm. Graphs of $20 \log_{10} |E_{1\rho}(\rho,0,0)|$ as a function of the radial distance ρ are shown in Fig. 2 at the frequencies $f = 5$, 10, and 20 GHz. Also shown are the separate magnitudes of the parts of the field due to the lateral wave alone and due to the direct wave alone. It is seen that in the vicinity of the radial distance where these two parts have

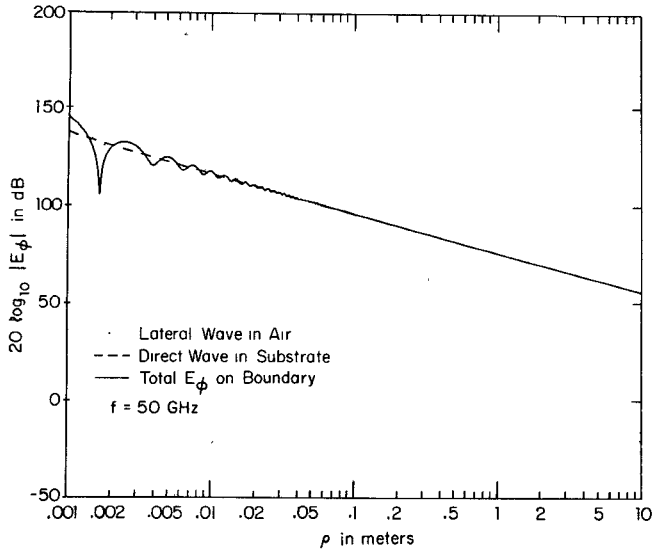

Fig. 3. Interference pattern of lateral- and direct-wave components of E_ϕ.

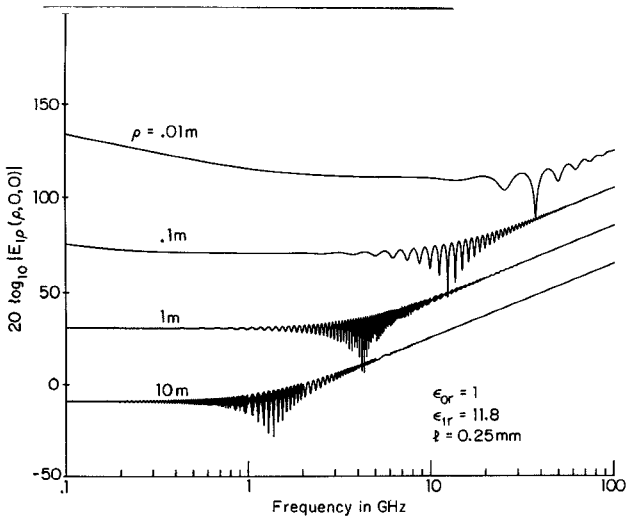

Fig. 4. Interference patterns between direct and lateral waves due to horizontal electric dipole on air–dielectric surface of microstrip.

equal magnitudes, sharp interference patterns occur. It is also clear that at distances beyond the point of intersection, the lateral wave dominates. A similar pattern for $E_{1\phi}(\rho, \pi/2, 0)$ is shown in Fig. 3 at $f = 50$ GHz. An alternative representation is in Fig. 4, where the frequency is the variable and the radial distance is the parameter. The shorter the radial distance to the point of observation, the higher the frequency at which interference occurs.

III. The Propagation of Pulses on Microstrip

A simple way in which to show the properties of microstrip under transient conditions is to superimpose a suitable set of frequencies that combine to form a well-shaped pulse [2]. This is illustrated in Fig. 5, which shows a pulse formed by the superposition of the following set of frequencies: 50 MHz to 50 GHz at 50 MHz intervals with Gaussian amplitude weighting. (Note that with $l = 0.25$ mm and $\epsilon_{1r} = 11.8$, the condition $k_1 l < 1$ is satisfied over

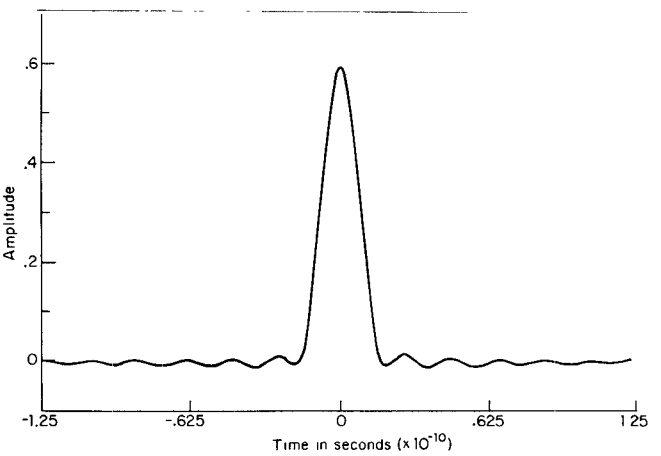

Fig. 5. Input signal: superposition of continuous-wave (CW) signals at 50 MHz intervals from 50 MHz to 50 GHz; Gaussian amplitude weighting. Taken from Gulla [2].

the entire range of frequencies.) The propagation of this pulse along the boundary between air and a dielectric half-space can be observed by evaluating the field due to the superposition of the same set of frequencies at successive radial distances. The results at four radial distances are shown in Fig. 6(a) and (b) when $\epsilon_{1r} = 11.8$. At the shortest radial distance (top in Fig. 6(a)), the component pulses due respectively to the superposition of the lateral waves in air and the direct waves in the dielectric are also shown. This separate evaluation is not necessary at larger distances from the source since the two pulses become separated because they have different velocities, viz., the velocity of light $c = 3 \times 10^8$ m/s in the air and the velocity $v = c\epsilon_{1r}^{-1/2}$ in the dielectric. Close to the source the lateral-wave pulse is much smaller than the direct-wave pulse. As the radial distance is increased, the lateral-wave pulse grows relative to the direct-wave pulse. Note that the two shapes are quite different: the direct-wave pulse corresponds closely to the initial pulse in Fig. 5; the lateral-wave pulse suggests the derivative of the initial pulse. The reason for these differences is explained later.

The same initial pulse can be applied to microstrip by the same procedure, viz., the evaluation of the field at successive distances due to the superposition of the fields generated at the selected set of frequencies. The initial pulse and the propagated pulse at different radial distances from the source are shown in Fig. 7(a) and (b) for a microstrip with a substrate of thickness $l = 0.25$ mm and a relative permittivity $\epsilon_{1r} = 11.8$. At the shortest radial distance the separate lateral-wave and direct-wave pulses are shown along with their superposition in the total transient field. The general behavior of the two pulses is quite similar to that along the two-layer region shown in Fig. 6(a) with certain significant differences. Most conspicuous is the shape of the lateral-wave pulse, which has an additional peak presumably due to reflection from the conducting base. There is no corresponding change in the direct-wave pulse. These differences are explained later. The lateral-wave pulse travels more rapidly than the direct-wave

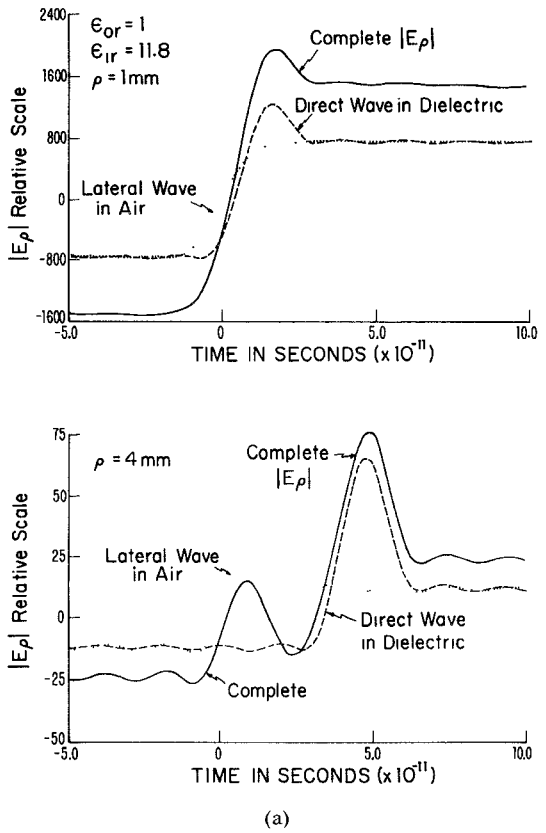

(a)

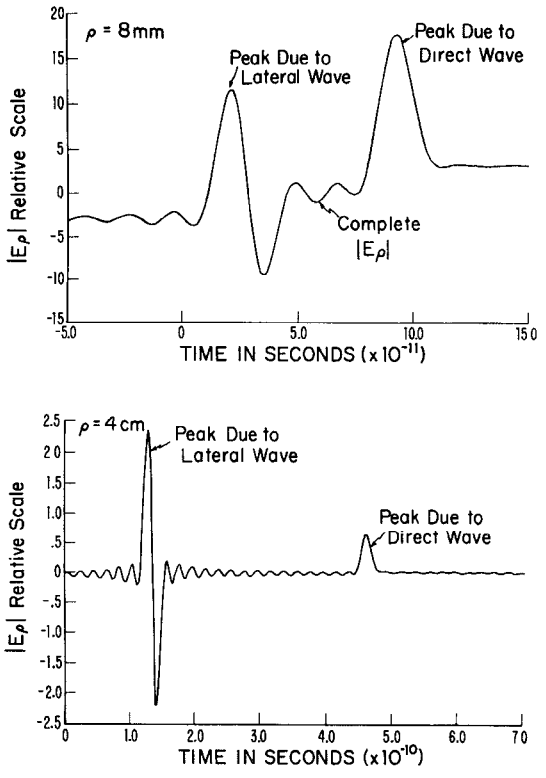

(b)

Fig. 6. Pulse propagating along air–dielectric boundary; data taken from Gulla [2]. (a) Top: $\rho = 1$ mm. Bottom: $\rho = 4$ mm. (b) Top: $\rho = 8$ mm. Bottom: $\rho = 4$ cm.

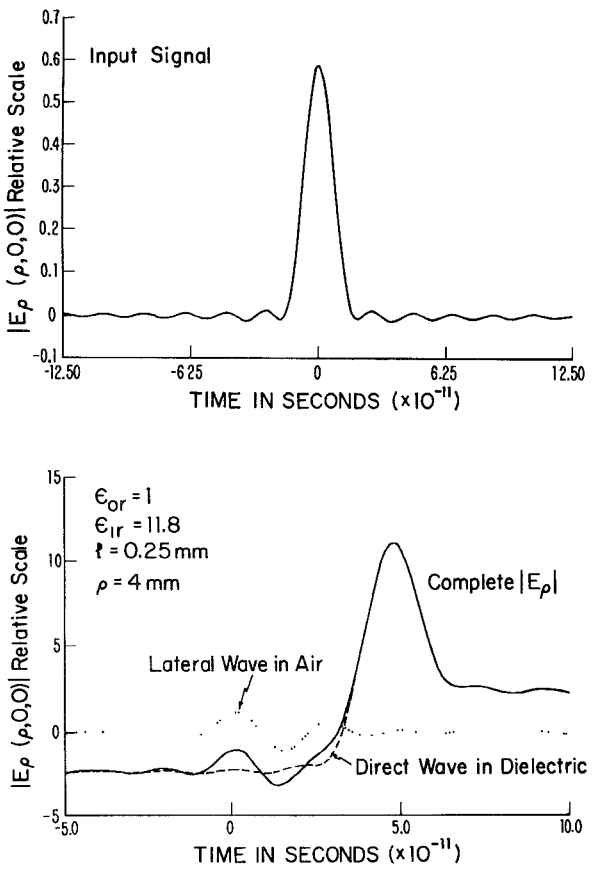

(a)

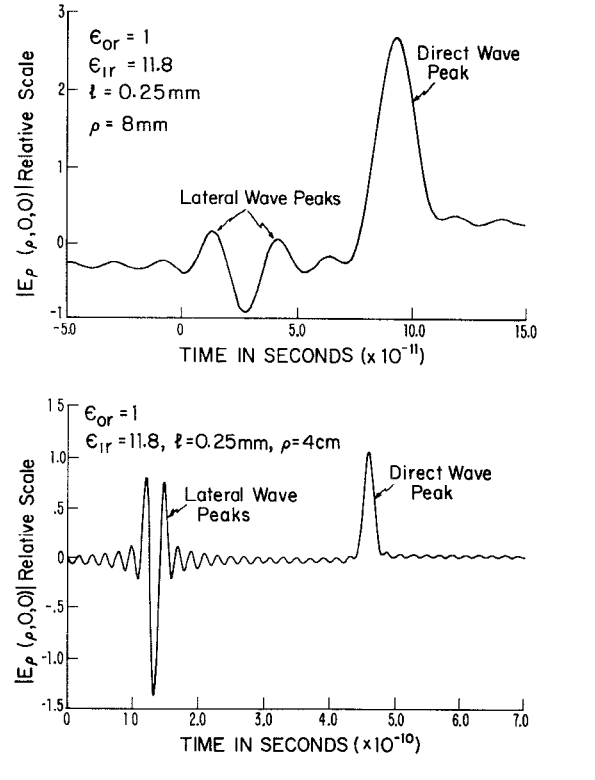

(b)

Fig. 7. Pulse propagating along microstrip; data taken from Gulla [2]. (a) Top: input signal. Bottom: $\rho = 4$ mm. (b) Top: $\rho = 8$ mm. Bottom: $\rho = 4$ cm.

pulse and arrives correspondingly earlier. For example, at $\rho = 4$ cm, the lateral-wave pulse arrives 3.45×10^{-10} s before the direct-wave pulse since the two velocities are $c = 3\times10^8$ m/s and $v = c/\sqrt{11.8} = 0.87\times10^8$ m/s.

IV. The Propagation of a Gaussian Pulse Along the Boundary Between Air and a Dielectric

In the preceding section the propagation of a single pulse along the boundary between air and a dielectric half-space and along the air–substrate surface of open microstrip is examined simply by the superposition of a selection of frequencies that together constitute a single pulse at the source point. A more fundamental alternative involves the derivation of explicit formulas for the propagation of pulses along these boundaries when the exciting source is a horizontal dipole located on the same boundaries. From such formulas an understanding can be gained of the reasons for the differences in the shapes of the pulses and their rates of decrease in amplitude with distance from the source.

In a recent paper [3] the transient electromagnetic field of a vertical electric dipole located on the boundary between two dielectric half-spaces is determined when the dipole is excited by a Gaussian current pulse. The corresponding field of a horizontal electric dipole is readily obtained [4] from that of the vertical dipole. The components of interest here are

$$E_{1z}(\rho,0,0;t) = -\frac{1}{2\pi\epsilon_0\epsilon^{3/2}}\frac{\pi^{-1/2}}{c^3t_1^3}\left\{\left[-\frac{2\tau'}{\rho_1}+\frac{1}{\rho_1^2}\right]e^{-\tau'^2} + \frac{e^{-T'^2/2}}{\sqrt{\epsilon\rho_1}}\begin{bmatrix}1.87V(0,\sqrt{2}\,T')-2.64T'V(-1,\sqrt{2}\,T')\\ 1.05U(0,-\sqrt{2}\,T')+2.90T'U(-1,-\sqrt{2}\,T')\end{bmatrix}\right\}\begin{matrix}T'\geq 0\\ T'\leq 0\end{matrix} \tag{2}$$

$$E_{1\rho}(\rho,0,0;t) = \frac{1}{2\pi\epsilon_0\epsilon}\frac{\pi^{-1/2}}{c^3t_1^3}\left\{\left[-\frac{2\tau'}{\rho_1}+\frac{1}{\rho_1^2}\right]e^{-\tau'^2} + \frac{\pi^{1/2}}{2\rho_1^3}(\operatorname{erf}\tau'+1)+\epsilon^{3/2}\left[\frac{e^{-\tau_\epsilon'^2}}{\rho_{1\epsilon}^2}+\frac{\pi^{1/2}}{2\rho_{1\epsilon}^3}(\operatorname{erf}\tau_\epsilon'+1)\right] + \frac{e^{-T'^2/2}}{\sqrt{\epsilon\rho_1}}\begin{bmatrix}1.87V(0,\sqrt{2}\,T')-2.64T'V(-1,\sqrt{2}\,T')\\ 1.05U(0,-\sqrt{2}\,T')+2.90T'U(-1,-\sqrt{2}\,T')\end{bmatrix}\right\}\begin{matrix}T'\geq 0\\ T'\leq 0\end{matrix} \tag{3}$$

where t_1 is the half-width of the normalized Gaussian pulse,

$$f(t) = \frac{e^{-t^2/t_1^2}}{t_1\sqrt{\pi}} \tag{4}$$

and

$$\rho_1 = \rho/ct_1 \qquad \rho_{1\epsilon} = \rho\epsilon^{1/2}/ct_1 \tag{5}$$

$$\tau' = (t-\rho/c)/t_1 = t'-\rho_1 \qquad \tau_\epsilon' = (t-\rho\epsilon^{1/2}/c)/t_1 = t'-\rho_{1\epsilon} \tag{6}$$

$$T' = \frac{t-\frac{\rho}{c}\left(1-\frac{1}{2\epsilon}\right)}{t_1}. \tag{7}$$

The functions V and U are the parabolic cylinder functions defined in [5].

The dominant parts of (2) and (3) are the same. They consist of the first square bracket which contains two terms. The second of these is a Gaussian pulse which decreases with radial distance from the source as $1/\rho^2$. The first term is the time derivative of the Gaussian pulse. It decreases with radial distance as $1/\rho$ so that it dominates except close to the source. This means that what starts as a Gaussian pulse quickly changes to a pulse shaped like the derivative. The two formulas also have in common the term with parabolic cylinder functions and an explicit $1/\sqrt{\rho}$ decrease with radial distance. Note, however, that ρ also occurs in the arguments of the parabolic cylinder functions. This entire term is significant only at large distances, where it approaches a $1/\rho^2$ dependence on the distance.

The expression (3) for $E_{1\rho}(\rho,0,0;t)$ includes a second Gaussian pulse which decreases as $1/\rho^2\epsilon$ and travels in the dielectric with the velocity $c\epsilon^{-1/2}$. It arrives later than the pulse in air and at even moderate radial distances it is much smaller. Also in (3) are two terms that involve the error function and that decrease with distance as $1/\rho^3$ and $1/\rho^3\epsilon^{3/2}$. They contribute to the initial rise of the pulse and give the entire static field that persists after both pulses have passed. Although not evident in (2) because of the

approximation involved in the steady-state formula, there is actually also a similar second pulse in the complete transient for $E_{1z}(\rho,0,0;t)$.

The transient field given by (2) and (3) for the dipole with Gaussian pulse excitation is in complete agreement with that determined by the superposition of a set of frequencies as detailed in Section III. The constructed pulse shown in Fig. 5 is not a Gaussian pulse but in its main peak is sufficiently like one so that the field generated by it closely resembles that of a Gaussian pulse. Since explicit formulas are available for the components of the field generated by a Gaussian pulse, these can be used to explain the properties of the field generated by the pulse shown in Fig. 5. In particular, the fact that the single pulse in Fig. 5 generates two field pulses of which the first is like the derivative of the generating pulse and the second is like the generating pulse itself is clarified by comparison with the formulas for the Gaussian pulse.

V. The Transient Electric Field Generated in Open Microstrip by a Horizontal Dipole Excited by a Gaussian Pulse

The steady-state formulas for the electric field generated by a horizontal electric dipole on the air–substrate surface of microstrip are given by (44) and (55) with $z=0$ in [1]. The Fresnel-integral term is omitted for simplicity since its contribution is important only at large distances. In the direction $\phi=0$ along the axis of the dipole, the components are

$$\tilde{E}_{1\rho}(\rho',0,0)=\frac{\mu_0}{2\pi\epsilon c}\left\{\frac{\epsilon^{1/2}l}{c}\left(-\frac{\omega^2}{\rho'}-\frac{i\omega}{\rho'^2}+\frac{1}{\rho'^3}\right)e^{i\omega\rho'}+\epsilon^{3/2}\left[2\left(\frac{1}{\rho_\epsilon'^2}+\frac{i}{\omega\rho_\epsilon'^3}\right)-\frac{\epsilon^{1/2}l}{c}\left(\frac{\omega}{\rho_\epsilon'^2}+\frac{i}{2\rho_\epsilon'^3}\right)\right]e^{i\omega\rho_\epsilon'}\right\} \quad (8)$$

$$\tilde{E}_{1z}(\rho',0,0)=\frac{\mu_0 l}{2\pi\epsilon c^2}\left(\frac{\omega^2}{\rho'}+\frac{i\omega}{\rho'^2}\right)e^{i\omega\rho'} \quad (9)$$

where l is the thickness of the substrate and

$$\rho'=\rho/c \qquad \rho_\epsilon'=\rho'\epsilon^{1/2}=\rho\epsilon^{1/2}/c. \quad (10)$$

When the dipole is excited by the normalized Gaussian pulse $f(t)$ with its Fourier transform $\tilde{f}(\omega)$, viz.,

$$f(t)=\frac{e^{-t^2/t_1^2}}{t_1\sqrt{\pi}} \qquad \tilde{f}(\omega)=e^{-\omega^2 t_1^2/4} \quad (11)$$

the transient field is given by

$$E_{1\rho}(\rho',0,0;t)=\frac{1}{2\pi}\operatorname{Re}\int_{-\infty}^{\infty}\tilde{E}_{1\rho}(\rho',0,0;\omega)e^{-\omega^2t_1^2/4}e^{-i\omega t}\,d\omega=\frac{\mu_0}{2\pi\epsilon c}\left[\frac{\epsilon^{1/2}l}{c}\left(-\frac{I_0}{\rho'}-\frac{I_1}{\rho'^2}+\frac{I_2}{\rho'^3}\right)+2\epsilon^{3/2}\left(\frac{I_{2\epsilon}}{\rho_\epsilon'^2}+\frac{I_{3\epsilon}}{\rho_\epsilon'^3}\right)\right] \quad (12)$$

where with

$$\tau=t-\rho' \qquad \tau_\epsilon=t-\rho_\epsilon' \quad (13)$$

and from [3, eqs. (51), (52), and (56)],

$$I_1=\operatorname{Re}\frac{1}{2\pi}\int_{-\infty}^{\infty}i\omega e^{-\omega^2t_1^2/4}e^{-i\omega\tau}\,d\omega=\frac{2\tau}{\sqrt{\pi}\,t_1^3}e^{-\tau^2/t_1^2}$$

$$I_{1\epsilon}=\frac{2\tau_\epsilon}{\sqrt{\pi}\,t_1^3}e^{-\tau_\epsilon^2/t_1^2} \quad (14)$$

$$I_2=\operatorname{Re}\frac{1}{2\pi}\int_{-\infty}^{\infty}e^{-\omega^2t_1^2/4}e^{-i\omega\tau}\,d\omega=\frac{1}{t_1\sqrt{\pi}}e^{-\tau^2/t_1^2}$$

$$I_{2\epsilon}=\frac{1}{t_1\sqrt{\pi}}e^{-\tau_\epsilon^2/t_1^2} \quad (15)$$

$$I_3=\operatorname{Re}\frac{1}{2\pi}\int_{-\infty}^{\infty}\frac{i}{\omega}e^{-\omega^2t_1^2/4}e^{-i\omega\tau}\,d\omega=\frac{1}{2}\left[1+\operatorname{erf}(\tau/t_1)\right]$$

$$I_{3\epsilon}=\frac{1}{2}\left[1+\operatorname{erf}(\tau_\epsilon/t_1)\right] \quad (16)$$

$$I_0=\operatorname{Re}\frac{1}{2\pi}\int_{-\infty}^{\infty}\omega^2e^{-\omega^2t_1^2/4}e^{-i\omega\tau}\,d\omega=\frac{dI_1}{dt}=\frac{2}{\sqrt{\pi}\,t_1^3}e^{-\tau^2/t_1^2}-\frac{4\tau^2}{\sqrt{\pi}\,t_1^5}e^{-\tau^2/t_1^2}. \quad (17)$$

Similarly,

$$E_{1z}(\rho',0,0;t)=\frac{1}{2\pi}\operatorname{Re}\int_{-\infty}^{\infty}\tilde{E}_{1z}(\rho',0,0;\omega)e^{-\omega^2t_1^2/4}e^{-i\omega t}\,d\omega=\frac{\mu_0 l}{2\pi\epsilon c^2}\left(\frac{I_0}{\rho'}+\frac{I_1}{\rho'^2}\right). \quad (18)$$

With the values for the integrals given above,

$$E_{1\rho}(\rho',0,0;t)=\frac{\mu_0}{2\pi\epsilon c}\frac{\epsilon^{1/2}l}{c}\left(-\frac{2}{\sqrt{\pi}\,t_1^3\rho'}+\frac{4\tau^2}{\sqrt{\pi}\,t_1^5\rho'}-\frac{2\tau}{\sqrt{\pi}\,t_1^3\rho'^2}+\frac{1}{\sqrt{\pi}\,t_1\rho'^3}\right)e^{-\tau^2/t_1^2}+\frac{\mu_0\epsilon^{3/2}}{2\pi\epsilon c}\left\{\frac{2e^{-\tau_\epsilon^2/t_1^2}}{\sqrt{\pi}\,t_1\rho_\epsilon'^2}+\frac{1}{\rho_\epsilon'^3}\left[1+\operatorname{erf}(\tau_\epsilon/t_1)\right]\right\} \quad (19)$$

$$E_{1z}(\rho',0,0;t)=\frac{\mu_0 l}{2\pi\epsilon c^2}\left(\frac{2}{\sqrt{\pi}\,t_1^3\rho'}-\frac{4\tau^2}{\sqrt{\pi}\,t_1^5\rho'}+\frac{2\tau}{\sqrt{\pi}\,t_1^3\rho'^2}\right)e^{-\tau^2/t_1^2}. \quad (20)$$

With the notation

$$\tau'=\tau/t_1 \qquad \tau_\epsilon'=\tau_\epsilon/t_1$$
$$\rho_1=\rho'/t_1=\rho/ct_1 \qquad \rho_{1\epsilon}=\rho_\epsilon'/t_1=\rho\epsilon^{1/2}/ct_1 \quad (21)$$

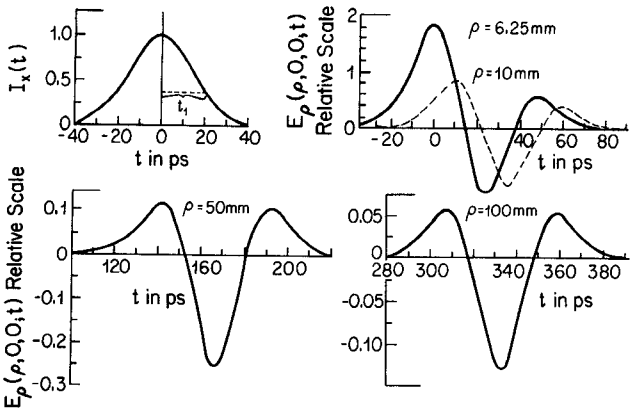

Fig. 8. Radial lateral-wave pulse on surface of microstrip with $l = 1.5$ mm, $\epsilon_{1r} = 13$, due to Gaussian current pulse with half-width $t_1 = 20.8$ ps in horizontal dipole on surface.

these formulas reduce to

$$E_{1\rho}(\rho,0,0;t)$$

$$= \frac{l}{2\pi\epsilon^{1/2}\epsilon_0}\frac{\pi^{-1/2}}{c^4 t_1^4}\left(-\frac{2}{\rho_1}+\frac{4\tau'^2}{\rho_1}-\frac{2\tau'}{\rho_1^2}+\frac{1}{\rho_1^3}\right)e^{-\tau'^2}$$

$$+\frac{\epsilon^{3/2}}{2\pi\epsilon\epsilon_0}\frac{\pi^{-1/2}}{c^3 t_1^3}\left[\frac{2}{\rho_{1\epsilon}^2}e^{-\tau_\epsilon'^2}+\frac{\pi^{1/2}}{\rho_{1\epsilon}^3}(1+\operatorname{erf}\tau_\epsilon')\right]$$

$$= -\frac{l}{2\pi\epsilon^{1/2}\epsilon_0}\frac{\pi^{-1/2}}{c^4 t_1^4}\left[\frac{2}{\rho_1}(1-2\tau'^2)+\frac{2\tau'}{\rho_1^2}-\frac{1}{\rho_1^3}\right]e^{-\tau'^2}$$

$$+\frac{\epsilon^{3/2}}{2\pi\epsilon\epsilon_0}\frac{\pi^{-1/2}}{c^3 t_1^3}\left[\frac{2}{\rho_{1\epsilon}^2}e^{-\tau_\epsilon'^2}+\frac{\pi^{1/2}}{\rho_{1\epsilon}^3}(1+\operatorname{erf}\tau_\epsilon')\right] \quad (22)$$

$$E_{1z}(\rho,0,0;t) = \frac{l}{\pi\epsilon\epsilon_0}\frac{\pi^{-1/2}}{c^4 t_1^4}\left[\frac{(1-2\tau'^2)}{\rho_1}+\frac{\tau'}{\rho_1^2}\right]e^{-\tau'^2}. \quad (23)$$

As in the two-layer formula, the second pulse of the form $\exp(-\tau_\epsilon'^2)/\rho_{1\epsilon}^2$ does not appear in the formula for $E_{1z}(\rho,0,0;t)$ because of the approximations involved in the frequency-dependent formula.

The Gaussian current pulse on the horizontal dipole is shown at the upper left in Fig. 8. It has the half-width $t_1 = 62.5/3 = 20.8$ ps. Following it is shown the radial electric-field pulse that occurs on the surface of the dielectric at distances of 6.25 mm and 10 mm. (Note that the exciting Gaussian current pulse has its central maximum at the reference time $t = 0$.) The pulse arrives at $\rho = 50$ mm at a later time and has the shape shown on the lower left in Fig. 8. The pulse at 100 mm is shown at the lower right. As soon as the $1/\rho$ term becomes dominant, the shape changes only slightly as the pulse advances with the velocity $c = 3\times10^8$ m/s.

The graphs in Fig. 8 show only the lateral-wave pulse because the time scale does not extend to the time of arrival of the direct-wave pulse. The complete field including both pulses is shown in Fig. 9, where the time scale is adjusted for each distance. At $\rho = 10$ mm, the lateral-wave pulse is relatively small compared to the direct-wave pulse

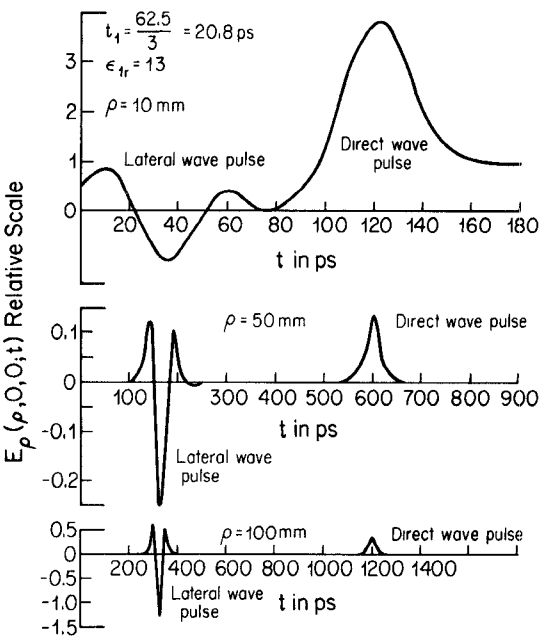

Fig. 9. Radial electric-field pulses on surface of open microstrip with $l = 1.5$ mm, $\epsilon_{1r} = 13$, due to Gaussian current pulse with half-width $t_1 = 20.8$ ps in horizontal dipole on surface.

which travels in the substrate with the slower velocity $v = c\epsilon_{1r}^{-1/2}$. At $\rho = 50$ mm, the pulses are of comparable size and already quite widely separated. At $\rho = 100$ mm, the direct-wave pulse is smaller than the lateral-wave pulse. The more rapid decrease of the direct-wave pulse with distance is a consequence of the fact that its radial dependence is $1/\rho^2$ whereas that of the leading term in the lateral-wave pulse is $1/\rho$.

The graphs in Figs. 8 and 9 showing the lateral-wave and direct-wave pulses generated on microstrip by a horizontal dipole excited by a Gaussian current pulse are consistent with the corresponding graphs in Fig. 7(a) and (b). The explicit formula (22) shows the underlying complexity of a lateral-wave pulse propagating along microstrip and the surprising analytical simplicity of the direct-wave pulse. It is interesting to inquire into the physical phenomena underlying these striking differences between the direct- and lateral-wave pulses.

The structure of microstrip provides the essential properties for the propagation of two very different types of surface waves. First, the boundary between air and a dielectric with quite large relative permittivity is the appropriate structure for the propagation of a lateral wave or pulse in the air. Second, the dielectric layer on a highly conducting plane is the essential medium for so-called "trapped" surface waves in the dielectric with an associated evanescent wave in the adjoining air. These were first analyzed by Attwood [6]; they are described in detail by Collin [7].

A horizontal electric dipole on the air–dielectric surface generates a lateral wave with all six components of the electromagnetic field. These are conveniently grouped as a lateral wave of electric (TM) type with cylindrical compo-

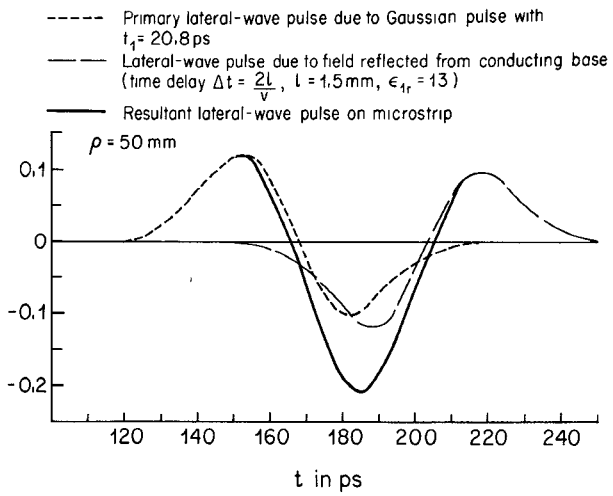

Fig. 10. Lateral-wave pulse on microstrip as superposition of pulse due to dipole and pulse due to field reflected from conducting base.

nents E_ρ, E_z, and B_ϕ, and a lateral wave of magnetic (TE) type with the components B_ρ, B_z, and E_ϕ. They have significant values in the air, on the boundary, and in the dielectric into which they travel from the air in a direction almost vertically downward. When a current pulse is impressed on the dipole, a lateral-wave electric-field pulse travels in the air to the point of observation at $\rho = L$. A similar pulse traveling down into the dielectric is reflected at the metal surface with a reversal in direction. It arrives at $\rho = L$ delayed by the extra time of travel over the distance $2l$ with the velocity $c\epsilon_{1r}^{-1/2}$. The two pulses and the single pulse resulting from their superposition are shown in Fig. 10 with $L = 50$ mm, $\epsilon_{1r} = 13$, and $t_1 = 20.8$ ps. The resultant pulse is seen to virtually duplicate the pulse for $\rho = 50$ mm in Fig. 8. Minor differences are due to small multiple reflections.

A horizontal electric dipole on the air–dielectric surface of microstrip can also generate "trapped" surface waves. These are of TM and TE types. The former have the components E_x (E_ρ with $\phi = 0$), E_z, and B_y (B_ϕ with $\phi = 0$); the latter, B_x, B_z, and E_y. The cutoff frequencies are defined by

$$\frac{2lf_c}{c} = \frac{2l}{\lambda_c} = \frac{n}{2\sqrt{\epsilon_{1r} - 1}}, \qquad n = 0,1,2,\cdots \tag{24}$$

where only odd TE modes and even TM modes are possible for a dielectric of thickness l on a conducting plane. Thus, only the TM_0 mode has no cutoff; the lowest possible TE mode, TE_1, has the cutoff frequency

$$f_c = \frac{c}{4l\sqrt{\epsilon_{1r} - 1}} = 14.4 \text{ GHz} \qquad \text{for } l = 1.5 \text{ mm}, \epsilon_{1r} = 13. \tag{25}$$

The three TM components of the direct-wave field in the dielectric are the same as the components of the TM_0 mode. At a distance $x = \rho = L$, the field on the surface $z = 0$ consists of a direct Gaussian pulse that travels the distance L and a TM_0 reflected pulse that traverses the zigzag distance $4\sqrt{(L/4)^2 + l^2} = \sqrt{L^2 + (4l)^2}$. With $L = 50$ mm and $l = 1.5$ mm, the zigzag path has a length 50.36 mm. The direction of the electric vector is reversed at each of two reflections at the metal surface and left unaltered by one perfect internal reflection at an angle greater than the critical angle at the air surface. Thus, the multiply reflected pulse arrives delayed by only 4.3 ps and with equal amplitude and the same shape at $\rho = L = 50$ mm, $z = 0$. The superposition of the two identical pulses that arrive almost at the same time yields a very slightly broadened direct pulse with doubled amplitude. This explains the factor 2 in the term for the direct-wave pulse in (22) as compared with the direct-wave pulse in (3). It also explains the nonappearance of the thickness of the dielectric in the formula for the direct-wave pulse. At distances $L \gg l$, there is no significant time delay and the TM_0 "trapped" pulse is multiply reflected without decrease in amplitude or change in shape.

The formulas for the electromagnetic field generated by a horizontal electric dipole on microstrip are derived from general integrals that include the lateral wave and all "trapped" surface waves in the dielectric. The condition $k_1 l < 1$ that is imposed in order to obtain simple formulas means that the multivalued $\tan k_1 l$ is replaced by $k_1 l$. In effect, this is equivalent to requiring the frequency to be low enough so that all higher "trapped" surface waves in the dielectric do not propagate. Thus, $k_1 l = \omega\epsilon_{1r}^{1/2} l/c < 1$ or $f < c/2\pi\epsilon_{1r}^{1/2} l$ is equivalent to $f < f_c$ where f_c is given by (25). With $\epsilon_{1r} = 13$ and $l = 1.5$ mm, $f < 8.8$ GHz $< f_c = 14.4$ GHz.

The range of frequencies with significant amplitudes in a Gaussian pulse of half-width t_1 is $\omega t_1 < 2.6$ or $f < 2.6/2\pi t_1$. With $t_1 = 20.8$ ps, $f < 20$ GHz. Since all frequencies in the pulse with large amplitudes are below f_c, none of the higher "trapped" surface-wave modes will propagate and contribute to the field in the dielectric.

VI. Microstrip Transmission Lines

A microstrip transmission line consists of a long metal strip of width w bonded directly to the surface of the substrate. In its simplest form, its thickness is small compared to the skin depth, so that currents are uniformly distributed through it. When the thickness is significantly greater than the skin depth, separate currents can be defined on the top and bottom surfaces of the strip and on its edges. Since each element of current is, in effect, a horizontal electric dipole, the field generated by the current along the entire length of the transmission line must consist of a suitable superposition of the fields of all the dipoles. This suggests that the physical meaning of the numerically determined currents in and electromagnetic field of specific microstrip transmission lines [8] should be illuminated by relating them to the fields of their dipole sources.

The complete frequency-dependent electric field on the surface of the air–substrate boundary due to a horizontal electric dipole is given in [1]. It consists of the components $E_\rho(\rho, \phi, 0)$, $E_\phi(\rho, \phi, 0)$, and $E_z(\rho, \phi, 0)$. Formulas for the

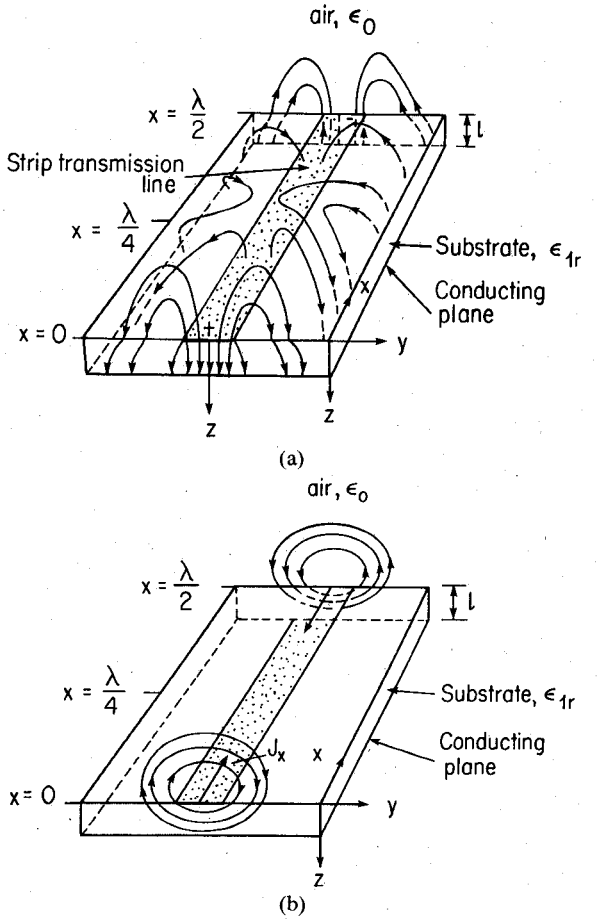

Fig. 11. (a) Electric-field lines in microstrip transmission line if this could support a pure TEM mode; $\lambda \equiv \lambda_{TEM}$ is distance between successive maxima. (b) Magnetic-field lines associated with electric field in Fig. 11(a).

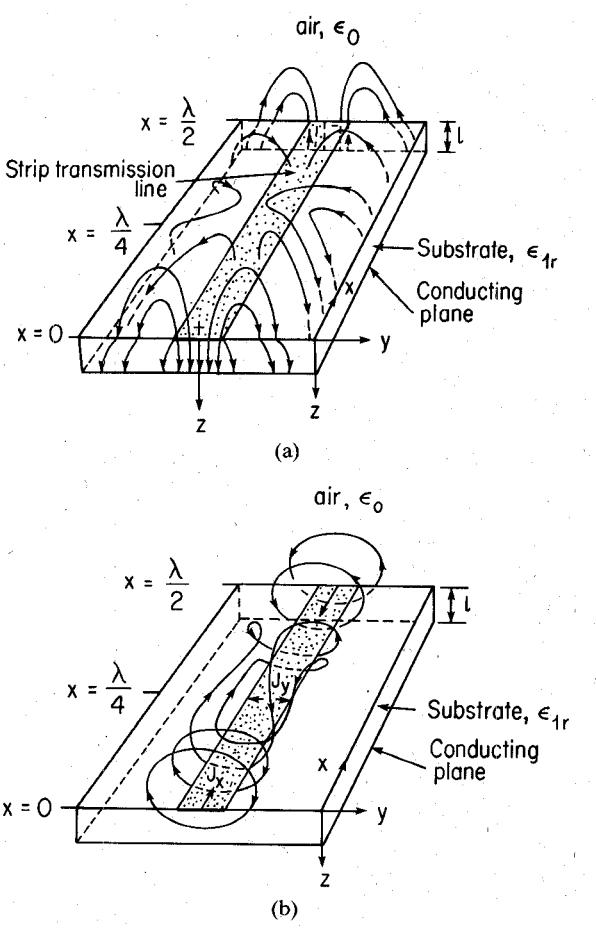

Fig. 12. (a) Electric-field lines in air and dielectric substrate generated by currents and charges in microstrip transmission line; λ is distance between successive maxima. (b) Magnetic-field lines associated with electric field in Fig. 12(a).

associated magnetic field are not given, but all three components $B_\rho(\rho,\phi,0)$, $B_\phi(\rho,\phi,0)$, and $B_z(\rho,\phi,0)$ are involved. Although not independent, the complete field consists of an electric (TM) part including E_ρ, E_z, and B_ϕ, and a magnetic part with B_ρ, B_z, and E_ϕ. Formulas for the field in the air above the boundary surface have not been derived, but the closely related field for the two-half-space problem is available [9]. It consists of a lateral wave that travels in the air near the boundary. Associated with it is a downward-traveling wave in the dielectric. Except quite close to the source, the electric-type components dominate because they decrease with radial distance as $1/\rho$ whereas the magnetic-type components decrease as $1/\rho^2$.

If a pure TEM mode could propagate in the x direction along a microstrip transmission line, the electric-field lines would have only E_y and E_z components that form loops that extend from the charges on the surfaces of the strip conductor to charges of opposite sign on the conducting base, as shown in Fig. 11(a). With a traveling wave along the line, there are cross-sectional planes at intervals of a wavelength $\lambda = 2\pi/k$ where the transverse electric field has a positive maximum. Halfway between these are negative maxima; i.e., the direction of the electric vector at each point in the plane is reversed. The electric field is zero at a quarter wavelength from a maximum. The associated magnetic field is also transverse. It forms closed loops around the strip conductor, as shown in Fig. 11(b). For a lossless line, the traveling-wave magnetic field is in phase with the electric field, so that the cross sections of maximum magnetic field coincide with the cross sections of maximum electric field.

A graph of the numerically evaluated electric field [8] of an actual microstrip transmission line is shown in Fig. 12(a). In the cross sections $x = 0, \lambda/2, \cdots$, where the magnitude of the transverse electric field is maximum, this is essentially like that of the TEM mode in Fig. 11. In these cross-sectional planes, the field is entirely transverse. However, it does not remain purely transverse in cross-sectional planes between these maxima. A longitudinal component E_x appears. It has its largest value in the planes $x = \lambda/4, 3\lambda/4, \cdots$, where $E_y = E_z = 0$. As shown in Fig. 12(a), the complete electric-field lines combine the three components E_x, E_y, and E_z. The loops formed by them include some for which one end terminates on the strip conductor, the other end on the conducting base; and loops that begin and end on the conducting base. The associated magnetic-field lines are shown in Fig. 12(b). In the planes $x = 0, \lambda/2$, the field is like that of the TEM line

in Fig. 11(b). Between these planes a longitudinal component of B appears and the magnetic lines form axially extended loops that link the currents in the strip twice—once in each direction.

The horizontal component E_x in the air is the lateral-wave component $E_\rho(\rho, 0, z)$ generated by all of the longitudinal currents in the strip. The lateral-wave components $E_z(\rho, 0, z)$ and $B_\phi(\rho, 0, z) = B_y$ combine with the components E_z and B_y of the TEM field. The lateral-wave component $B_\rho(\rho, \pi/2, z) = B_x$ provides the longitudinal magnetic field that occurs in Fig. 12(b). The lateral-wave components $B_z(\rho, \pi/2, z)$ and $E_\phi(\rho, \pi/2, z) = E_y$ combine with the TEM components B_z and E_y. The complete field in the air above a microstrip transmission line can be regarded as a suitably proportioned combination of the TEM field E_y, E_z and B_y, B_z with the lateral-wave field E_x, E_y, E_z and B_x, B_y, B_z. This combination is, of course, complicated by the different phase velocities for the lateral-wave and the TEM components. The effect is to make the combination—the quasi-TEM mode—frequency dependent.

It is perhaps well to point out that any "trapped" surface-wave modes that may exist in the dielectric can contribute nothing significant to the field in air because they are evanescent there. The entire field in the air is due to the superposition of all of the lateral-wave and TEM components generated by the current elements in the transmission line.

VII. Gaussian Pulse Propagation on an Open Microstrip Transmission Line

It is shown in Section V that a horizontal electric dipole located on the surface of microstrip and excited by a Gaussian current pulse generates an electric field outward along the axis of the dipole that consists of a lateral-wave pulse that travels in the air with the velocity of light and a slower direct-wave pulse that travels in the dielectric. The shapes of these pulses are shown in Figs. 8 and 9. A Gaussian current pulse applied at one end of a microstrip transmission line not only generates a field like that described above, but also moves along the strip conductor with the velocity of a TEM wave. The radial electric field that travels along the conductor induces a current in it. It follows that at a given point along the transmission line, the arrival of the Gaussian current pulse is preceded by the superposition of all of the currents induced by the radial electric field that is generated continuously by the approaching pulse. At successive distances this has the forms and relative amplitudes shown in Fig. 8. The pulse that is actually observed at the given point is the superposition of all of the induced currents and the currents that constitute the original pulse. This composite pulse is spread out over a much longer time than the original Gaussian and its shape is determined in no small measure by the distribution in time of the radial electric field at the point of observation.

Such a pulse has been calculated by Leung and Balanis [10] by first determining the "effective" wavenumber $k(\omega)$

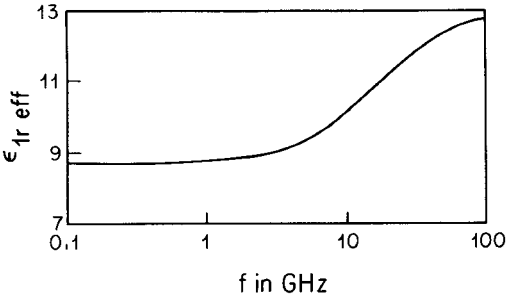

Fig. 13. Effective permittivity of microstrip with $\epsilon_{1r} = 13$, $l = 1.5$ mm; taken from Leung and Balanis [10].

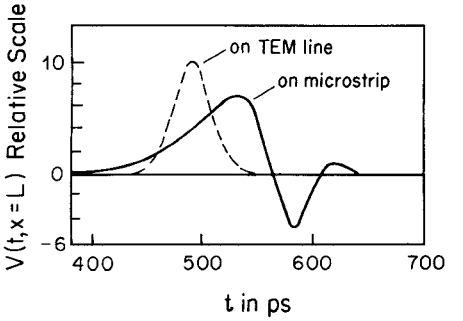

Fig. 14. Pulse at $x = 50$ mm due to Gaussian pulse with half-width $t_1 = 20$ ps at $x = 0$; taken from Leung and Balanis [10].

$= (\omega/c)\sqrt{\epsilon_{1r\text{eff}}(\omega)}$ by the spectral-domain method. The effective permittivity $\epsilon_{1r\text{eff}}(\omega)$ as evaluated by them as a function of the frequency is shown in Fig. 13 for a substrate with the thickness $l = 1.5$ mm and a relative permittivity $\epsilon_{1r} = 13$. A Gaussian voltage pulse $V(t, x = 0)$ with a half-width $t_1 = 20$ ps applied to the microstrip transmission line at $x = 0$ is next substituted in

$$V(t, x = L) = \frac{1}{2\pi}\int_{-\infty}^{\infty} \tilde{V}(\omega, x = 0)\, e^{j[\omega t - k(\omega)L]}\, d\omega \quad (26)$$

to determine the voltage pulse at $x = L$. In (26), $\tilde{V}(\omega, x = 0)$ is the Fourier transform of the Gaussian voltage $V(t, x = 0)$. A graph of the pulse $V(t, x = L)$ with $L = 50$ mm as computed from (26) by Leung and Balanis is shown in Fig. 14. Also shown in dotted line is the pulse that would arrive at $x = L$ if the line supported only the pure TEM mode with the wavenumber $k = (\omega/c)\sqrt{\epsilon_{1r\text{eff static}}}$, where $\epsilon_{1r\text{eff static}}$ is the effective static permittivity of the line.

In Fig. 14, the center of the Gaussian pulse on the TEM line arrives at $x = 50$ mm after $t = 490$ ps—the correct length of time to traverse 50 mm at the velocity $v = c/\sqrt{\epsilon_{1r\text{eff static}}}$ where $\epsilon_{1r\text{eff static}} = 8.65$. It is seen that a significant part of the actual pulse arrives earlier than any part of the Gaussian pulse and a major part later. The actual pulse is spread out over a much greater time interval than the Gaussian and its shape is very different. A comparison with Fig. 8 shows that its shape is actually very much like that of the radial electric field close to the source dipole, e.g., at $\rho = 6.25$ mm. Clearly the longitudinal lateral-wave electric field is of major importance in pulse propagation on microstrip transmission lines. It provides the long-range collinear coupling among the current elements that does not exist in a TEM line.

Results similar to those of Leung and Balanis [10] have been obtained by other authors [11], [12]. Notably the numerically calculated propagation of a Gaussian pulse in Fig. 3 of Li *et al.* [11] is represented by curves like those in Fig. 14 and closely resembling the changes in pulse shape with increasing distance of travel shown in Fig. 8 for a lateral-wave pulse.

VIII. Conclusion

A detailed analysis of the transmission of the electromagnetic waves and pulses generated by a horizontal electric dipole on the surface of a dielectric-coated conducting plane has been carried out. Relatively simple formulas have been derived for the three components of the electric field on the surface of the dielectric. The coexistence of a lateral wave and a direct wave leads to interference patterns in the frequency domain and a succession of two pulses with quite different shapes in the time domain. The significance of the lateral wave in providing strong long-range coupling among collinear elements in wave and pulse propagation along microstrip transmission lines has been demonstrated. Its existence is not obvious in numerical analyses such as the spectral-domain method, although its properties are necessarily included in any approach to microstrip that accurately satisfies the boundary conditions.

References

[1] R. W. P. King, "The propagation of signals along a three-layered region: Microstrip," *IEEE Trans. Microwave Theory Tech.*, vol. 36, pp. 1080–1086, June 1988.

[2] D. Gulla, "Surface electric field and transient signals along IC interconnects," master's thesis, Dept. Electrical Engineering, Tufts University, Medford, MA, Nov. 1988.

[3] R. W. P. King, "Lateral electromagnetic pulses generated by a vertical dipole on a plane boundary between dielectrics," *J. Electromagn. Waves Appl.*, vol. 2, pp. 225–243, 1988.

[4] R. W. P. King, "Lateral electromagnetic pulses generated on a plane boundary between dielectrics by vertical and horizontal dipole sources with Gaussian pulse excitation," *J. Electromagn. Waves Appl.*, to be published.

[5] M. Abramowitz and I. A. Stegun, *Handbook of Mathematical Functions*. New York: Dover, 1972.

[6] S. S. Attwood, "Surface-wave propagation over a coated plane conductor," *J. Appl. Phys.*, vol. 22, pp. 504–509, Apr. 1951.

[7] R. E. Collin, *Field Theory of Guided Waves*. New York: McGraw-Hill, 1960, pp. 461–465, 470–477.

[8] R. K. Hoffmann, *Handbook of Microwave Integrated Circuits*. Norwood, MA: Artech House, 1987, pp. 135–138.

[9] R. W. P. King, M. Owens, and T. T. Wu, "Properties of lateral electromagnetic fields and their application," *Radio Sci.*, vol. 21, pp. 13–23, Jan.–Feb. 1986.

[10] T. Leung and C. A. Balanis, "Pulse dispersion distortion in open and shielded microstrips using the spectral-domain method," *IEEE Trans. Microwave Theory Tech.*, vol. 36, pp. 1223–1226, July 1988.

[11] K. K. Li, G. Arjavalingham, A. Dienes, and J. R. Whinnery, "Propagation of picosecond pulses on microwave striplines," *IEEE Trans. Microwave Theory Tech.*, vol. MTT-30, pp. 1270–1273, Aug. 1982.

[12] J. F. Whitaker, T. B. Norris, G. Mourou, and T. Y. Hsiang, "Pulse dispersion and shaping in microstrip lines," *IEEE Trans. Microwave Theory Tech.*, vol. MTT-35, pp. 41–48, Jan. 1987.

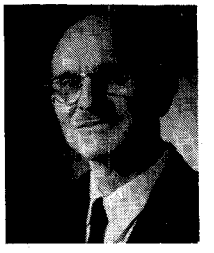

Ronold W. P. King (A'30–SM'43–F'53–LF'71) was born in Williamstown, MA, on September 19, 1905. He received the B.A. and M.S. degrees in physics from the University of Rochester, Rochester, NY, in 1927 and 1929, respectively, and the Ph.D. degree from the University of Wisconsin, Madison, in 1932, after having done graduate work at the University of Munich, Munich, Germany, and at Cornell University, Ithaca, NY.

He served as a Teaching and Research Assistant at the University of Wisconsin from 1932 to 1934, and as an Instructor and Assistant Professor of Physics at Lafayette College, Easton, PA, from 1934 to 1937. During the academic year 1937–1938 he was a Guggenheim Fellow in Germany. In 1938 he joined the faculty of Harvard University, Cambridge, MA.

Dr. King was Gordon McKay Professor of Applied Physics at Harvard from 1946 to 1972, when he became Gordon McKay Professor of Applied Physics, Emeritus. He was again a Guggenheim Fellow in 1958. He is a fellow of the American Physical Society and the American Academy of Arts and Sciences, a corresponding member of the Bavarian Academy of Sciences, and a member of the American Association for the Advancement of Science, Commission B of the International Scientific Radio Union, Phi Beta Kappa, and Sigma Xi. He is the author or coauthor of ten books, numerous articles in books and encyclopedias, and over 250 original papers in technical journals.